10720 *Inorg. Chem.* **2009**, *48*, 10720–10725
DOI: 10.1021/ic901477m

Inorganic Chemistry
Article

Electronic Structure and Spectroscopy of $[Ru(tpy)_2]^{2+}$, $[Ru(tpy)(bpy)(H_2O)]^{2+}$, and $[Ru(tpy)(bpy)(Cl)]^{+}$

Elena Jakubikova, Weizhong Chen, Dana M. Dattelbaum, Francisca N. Rein, Reginaldo C. Rocha,* Richard L. Martin, and Enrique R. Batista*

Los Alamos National Laboratory, Los Alamos, New Mexico 87545

Received July 24, 2009

We use a combined, theoretical and experimental, approach to investigate the spectroscopic properties and electronic structure of three ruthenium polypyridyl complexes, $[Ru(tpy)_2]^{2+}$, $[Ru(tpy)(bpy)(H_2O)]^{2+}$, and $[Ru(tpy)(bpy)(Cl)]^{+}$ (tpy = 2,2′:6′,2″-terpyridine and bpy = 2,2′-bipyridine) in acetone, dichloromethane, and water. All three complexes display strong absorption bands in the visible region corresponding to a metal-to-ligand-charge-transfer (MLCT) transition, as well as the emission bands arising from the lowest lying ^{3}MLCT state. $[Ru(tpy)(bpy)(Cl)]^{+}$ undergoes substitution of the Cl^- ligand by H_2O in the presence of water. Density functional theory (DFT) calculations demonstrate that the triplet potential energy surfaces of these molecules are complicated, with several metal-centered (^{3}MC) and ^{3}MLCT states very close in energy. Solvent effects are included in the calculations via the polarizable continuum model as well as explicitly, and it is shown that they are critical for proper characterization of the triplet excited states of these complexes.

Introduction

Ruthenium polypyridyl complexes comprise a versatile class of compounds with unique electrochemical and photophysical properties. They are widely used as oxidation catalysts,[1,2] photocatalysts[3] and dye sensitizers for solar cells.[4,5] In this work we characterize the spectroscopic properties and electronic structure of three complexes: $[Ru(tpy)_2]^{2+}$, $[Ru(tpy)(bpy)(H_2O)]^{2+}$, and $[Ru(tpy)(bpy)(Cl)]^{+}$.

Ruthenium(II) terpyridine derivatives are often used as building blocks in molecular assemblies[6,7] as well as dye sensitizers[8−10] because of their advantageous linear structural directionality compared to bipyridine derivatives. An interesting aspect of the $[Ru(tpy)_2]^{2+}$ photochemistry is its anomalously weak emission at the room temperature in comparison to other ruthenium polypyridyl complexes. For example, the triplet state lifetime of $[Ru(bpy)_3]^{2+}$ in aqueous solution at room temperature is 2500 times longer than the lifetime of $[Ru(tpy)_2]^{2+}$ at the same conditions, 620 ns[3] versus 250 ps,[11] respectively. A widely accepted explanation for this anomalously short lifetime and weak emission in $[Ru(tpy)_2]^{2+}$ is thermally activated crossing from the lowest triplet metal-to-ligand-charge-transfer (^{3}MLCT) state to a short-lived metal-centered (^{3}MC) state. The ^{3}MC state then non-radiatively relaxes into the ground state.[11] Recently, Borg et al.[12] used density functional theory (DFT) to investigate the potential energy surface of $[Ru(tpy)_2]^{2+}$ and related complexes. Their study determined that, in vacuum, the ^{3}MC state for $[Ru(tpy)_2]^{2+}$ is lower in energy than the ^{3}MLCT state by about 4 kcal/mol. Calculations including solvent effects on the relative stabilities of these two states were not reported in their work.

$[Ru(tpy)(bpy)(O)]^{2+}/[Ru(tpy)(bpy)(H_2O)]^{2+}$ is a catalytic system for the oxidation of alcohols, aldehydes, and unsaturated hydrocarbons.[13−17] In the catalytic process,

*To whom correspondence should be addressed. E-mail: erb@lanl.gov (E. R.B.), rcrocha@lanl.gov (R.C.R.).

(1) Rodriguez, M.; Romero, I.; Sens, C.; Llobet, A. *J. Mol. Catal. A: Chem.* **2006**, *251*, 215–220.
(2) Meyer, T. J.; Huynh, M. H. V. *Inorg. Chem.* **2003**, *42*, 8140–8160.
(3) Roundhill, D. M., Photochemistry, photophysics, and photoredox reactions of $Ru(bpy)_3^{2+}$ and related complexes. In *Photochemistry and photophysics of metal complexes*; Plenum Press: New York, 1994; pp 165−215.
(4) O'Regan, B.; Gratzel, M. *Nature* **1991**, *353*, 737–740.
(5) Hagfeldt, A.; Gratzel, M. *Chem. Rev.* **1995**, *95*, 49–68.
(6) Constable, E. C. *Chem. Soc. Rev.* **2007**, *36*, 246–253.
(7) Hofmeier, H.; Schubert, U. S. *Chem. Soc. Rev.* **2004**, *33*, 373–399.
(8) Houarner-Rassin, C.; Chaignon, F.; She, C.; Stockwell, D.; Blart, E.; Buvat, P.; Lian, T.; Odobel, F. *J. Photochem. Photobiol., A* **2007**, *192*, 56.
(9) Houarner-Rassin, C.; Blart, E.; Buvat, P.; Odobel, F. *J. Photochem. Photobiol., A* **2007**, *186*, 135.
(10) Beley, M.; Bignozzi, C. A.; Kirsch, G.; Alebbi, M.; Raboin, J. C. *Inorg. Chim. Acta* **2001**, *318*, 197.
(11) Sauvage, J. P.; Collin, J. P.; Chambron, J. C.; Guillerez, S.; Coudret, C.; Balzani, V.; Barigelletti, F.; Decola, L.; Flamigni, L. *Chem. Rev.* **1994**, *94*, 993–1019.
(12) Borg, O. A.; Godinho, S.; Lundqvist, M. J.; Lunell, S.; Persson, P. *J. Phys. Chem. A* **2008**, *112*, 4470–4476.
(13) Thompson, M. S.; Degiovani, W. F.; Moyer, B. A.; Meyer, T. J. *J. Org. Chem.* **1984**, *49*, 4972–4977.
(14) Thompson, M. S.; Meyer, T. J. *J. Am. Chem. Soc.* **1982**, *104*, 5070–5076.
(15) Moyer, B. A.; Thompson, M. S.; Meyer, T. J. *J. Am. Chem. Soc.* **1980**, *102*, 2310–2312.
(16) Farrer, B. T.; Thorp, H. H. *Inorg. Chem.* **1999**, *38*, 2497–2502.

 Published on Web 10/20/2009

$[Ru^{IV}(tpy)(bpy)(O)]^{2+}$ is reduced to the resting state $[Ru^{II}(tpy)(bpy)(H_2O)]^{2+}$, which can then undergo a two step proton-coupled oxidation to the active state $[Ru^{IV}(tpy)(bpy)(O)]^{2+}$:

$$[Ru^{II}(tpy)(bpy)(H_2O)]^{2+} \rightarrow [Ru^{III}(tpy)(bpy)(OH)]^{2+} + e^- + H^+ \quad (1)$$

$$[Ru^{III}(tpy)(bpy)(OH)]^{2+} \rightarrow [Ru^{IV}(tpy)(bpy)(O)]^{2+} + e^- + H^+ \quad (2)$$

Because $[Ru(tpy)(bpy)(Cl)]^+$ is obtained as a precursor of $[Ru(tpy)(bpy)(H_2O)]^{2+}$ and related $[Ru(tpy)(bpy)(L)]^{n+}$ complexes, its redox and spectroscopic properties are worthy of comparison with $[Ru(tpy)_2]^{2+}$ in this series. In this work we perform a joint experimental and theoretical characterization of the electronic structure and spectroscopy of these molecules in three different solvents: dichloromethane, acetone, and water.

Methods

Experimental Methods. $[Ru(tpy)_2](PF_6)_2$,[18] $[Ru(tpy)(bpy)(Cl)](PF_6)$,[19] and $[Ru(tpy)(bpy)(H_2O)](ClO_4)_2$[19] were prepared and characterized as described in the literature. High-purity acetone and dichloromethane were distilled and dried prior to use. Aqueous solutions were prepared using deionized water from a Nanopure purification system.

UV−vis absorption spectra were recorded using an HP 8452 diode-array spectrophotometer at a resolution of 2 nm. The measurements were performed by dissolving the complexes in the solvents of interest such that the maximum of the MLCT absorption in the visible region was <0.25 absorbance unit, which results in typical solute concentrations of 1×10^{-5} M.

Emission spectra were collected using a PTI Quantamaster Spectrofluorometer with Xenon excitation source. For the measurements, a small quantity of the complex was dissolved in the solvent of interest at a concentration to give a maximum for the visible MLCT band of 0.1−0.2 absorbance unit. The solutions were deaerated by sparging with N_2 for at least 15−20 min. Excitation wavelengths ranged from 400 to 500 nm, with detection using either a PMT or an InGaAs detector. Raman peaks corresponding to intense C−H stretching modes (near 2900 cm^{-1}) were detected and removed from the spectra. All spectroscopic data reported herein were obtained at the room temperature.

Computational Methods. DFT calculations were performed at the B3LYP[20,21] level of theory, using the SDD relativistic effective core potential with its associated triple-ζ basis set[22] on the Ru metal center and the 6-31G* basis set[23,24] on all other atoms. Ground-state geometries of all molecules were optimized in vacuum. To study the ground-state electronic structure in different solvents, a series of single point calculations were performed at the vacuum-optimized geometries, in which solvent effects were introduced via the polarizable continuum solvation model (PCM).[25]

To ensure that the ground-state vacuum-optimized geometries were adequate for performing single point calculations in different solvents, the ground-state geometry of $[Ru(tpy)_2]^{2+}$ was optimized in acetone. The resulting ground-state geometry, electronic structure, absorption spectra in acetone, and vibrational frequencies were virtually identical to those of the vacuum-optimized molecules, thereby justifying the use of vacuum-optimized geometry to study the ground-state electronic structure and absorption spectra of these molecules.

Time dependent DFT (TD-DFT) calculations[26−28] were performed on all three complexes in the visible spectral region (approximately 400−700 nm) in acetone, dichloromethane, and water. Solvent effects were introduced via the PCM. Natural transition orbital (NTO) analysis[29] was carried out to better understand the results of TD-DFT calculations. The absorption spectra were simulated by convoluting the spectrum composed of the δ-functions at the excitation energies times the oscillator strengths with a Lorentzian line-shape with the half width at half-maximum (hwhm) equal to 0.2 eV. The hwhm was chosen so as to achieve the best match between the experimental and calculated spectra.

Emission spectra were calculated using the fully optimized geometries of ground state and ^{3}MLCT excited state. The energy of the $0 \rightarrow 0$ transition was obtained as a difference between the energies of ground and excited states. The shape of the overall vibrational envelope was calculated by the use of Franck−Condon integrals, which describe the overlap between vibrational wave functions of ground and excited states. The magnitude of Franck−Condon integrals was determined using Huang−Rhys factors computed from geometry changes between ground and excited states along the ground state vibrational modes.[30,31] The hwhm values were set to 0.08 eV for $[Ru(tpy)(bpy)(Cl)]^+$ and 0.10 eV for $[Ru(tpy)(bpy)(H_2O)]^{2+}$, to achieve the best match between the experimental and calculated spectra.

The molecular geometries for the triplet states were obtained via a full self-consistent field (SCF) optimization. Solvent effects were included as a reaction field using the PCM methodology, as well as explicitly for the $[Ru(tpy)(bpy)(H_2O)]^{2+}$ molecule by considering two H_2O solvent molecules directly bound to the H_2O ligand. Unlike in the case of the ground-state optimizations, inclusion of solvent effects in the excited-state optimizations proved important for our ability to obtain fully optimized geometries of triplet excited states with different character (i.e., ^{3}MC as well as ^{3}MLCT). Frequency calculations were performed to confirm that the minimum was found for all optimized structures. Radii from the UFF force field[32] were used in all PCM calculations.

All calculations, except for the simulation of emission spectra and triplet-state geometry optimizations of $[Ru(tpy)(bpy)(H_2O)]^{2+}$,

(17) Madurro, J. M.; Chiericato, G., Jr.; F., D. G. W.; Romero, J. S. *Tetrahedron Lett*. **1988**, *29*, 765.
(18) Constable, E. C.; Cargill Thompson, D. W.; Tocher, D. A.; Daniels, M. A. M. *New J. Chem*. **1992**, *16*, 855–867.
(19) Takeuchi, K. J.; Thompson, M. S.; Pipes, D. W.; Meyer, T. J. *Inorg. Chem*. **1984**, *23*, 1845–1851.
(20) Becke, A. D. *J. Chem. Phys*. **1993**, *98*, 5648–52.
(21) Stephens, P. J.; Devlin, F. J.; Chabalowski, C. F.; Frisch, M. J. *J. Phys. Chem*. **1994**, *98*, 11623–11627.
(22) Andrae, D.; Haussermann, U.; Dolg, M.; Stoll, H.; Preuss, H. *Theor. Chim. Acta* **1990**, *77*, 123–141.
(23) Hehre, W. J.; Ditchfield, R.; Pople, J. A. *J. Chem. Phys*. **1972**, *56*, 2257–61.
(24) Harihara, P. C.; Pople, J. A. *Theor. Chim. Acta* **1973**, *28*, 213–22.
(25) Cossi, M.; Scalmani, G.; Rega, N.; Barone, V. *J. Chem. Phys*. **2002**, *117*, 43–54.
(26) Stratmann, R. E.; Scuseria, G. E.; Frisch, M. J. *J. Chem. Phys*. **1998**, *109*, 8218–8224.
(27) Bauernschmitt, R.; Ahlrichs, R. *Chem. Phys. Lett*. **1996**, *256*, 454–464.
(28) Casida, M. E.; Jamorski, C.; Casida, K. C.; Salahub, D. R. *J. Chem. Phys*. **1998**, *108*, 4439–4449.
(29) Martin, R. L. *J. Chem. Phys*. **2003**, *118*, 4775–4777.
(30) Cornil, J.; Beljonne, D.; Shuai, Z.; Hagler, T. W.; Campbell, I.; Bradley, D. D. C.; Bredas, J. L.; Spangler, C. W.; Mullen, K. *Chem. Phys. Lett*. **1995**, *247*, 425–432.
(31) Tretiak, S.; Saxena, A.; Martin, R. L.; Bishop, A. R. *Phys. Rev. Lett*. **2002**, *89*, 097402–097404.
(32) Rappe, A. K.; Casewit, C. J.; Colwell, K. S.; Goddard, W. A.; Skiff, W. M. *J. Am. Chem. Soc*. **1992**, *114*, 10024–10035.

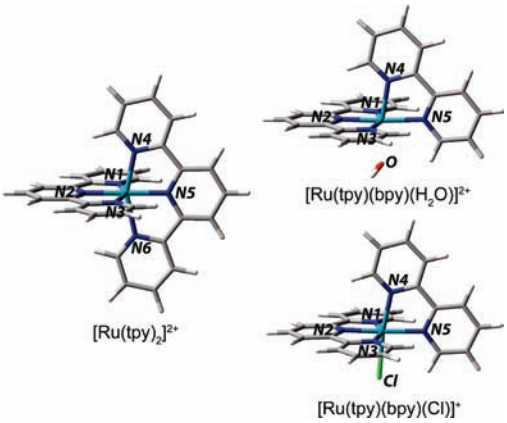

Figure 1. Ground state optimized geometries of $[Ru(tpy)_2]^{2+}$, $[Ru(tpy)(bpy)(H_2O)]^{2+}$, and $[Ru(tpy)(bpy)(Cl)]^{+}$.

were performed with the Gaussian 03 program package.[33] Gaussian 09[34] was employed to optimize the triplet states of $[Ru(tpy)(bpy)(H_2O)]^{2+}$ and $\{[Ru(tpy)(bpy)(H_2O)]^{2+}\} + 2H_2O$ (i.e., adduct with the explicit addition of two H_2O solvent molecules). Gaussian 09 implements an improved solvation model,[35,36] which made it possible to obtain fully optimized geometries for all triplet states of molecules with (H_2O) and $(H_2O) + 2H_2O$ ligands. While the total energies obtained with the Gaussian 03 and Gaussian 09 packages using the PCM model are significantly different, we found that the relative energies of different triplet states considered in this work are maintained within 0.5 kcal/mol.

Results and Discussion

A. Ground State Electronic Structure. Figure 1 shows the optimized geometries of $[Ru(tpy)_2]^{2+}$, $[Ru(tpy)(bpy)(H_2O)]^{2+}$, and $[Ru(tpy)(bpy)(Cl)]^{+}$. All three complexes have singlet multiplicity in their ground state and display pseudo-octahedral geometry about the Ru(II) center. The terpyridine and bipyridine groups are almost completely planar. Distances between Ru metal and coordinating atoms are given in Table 1 (full coordinates are provided in the Supporting Information).

Table 1. Bond Distances (Å) around Ru(II) for $[Ru(tpy)_2]^{2+}$, $[Ru(tpy)(bpy)(H_2O)]^{2+}$, and $[Ru(tpy)(bpy)(Cl)]^{+}$

bond lengths [Å]	$[Ru(tpy)_2]^{2+}$	$[Ru(tpy)(bpy)(H_2O)]^{2+}$	$[Ru(tpy)(bpy)(Cl)]^{+}$
Ru−N1(tpy)	2.12	2.12	2.10
Ru−N2(tpy)	2.01	2.00	1.98
Ru−N3(tpy)	2.12	2.12	2.10
Ru−N4(tpy/bpy)	2.12	2.06	2.09
Ru−N5(tpy/bpy)	2.01	2.11	2.12
Ru−N6(tpy)	2.12		
Ru−O		2.22	
Ru−Cl			2.42

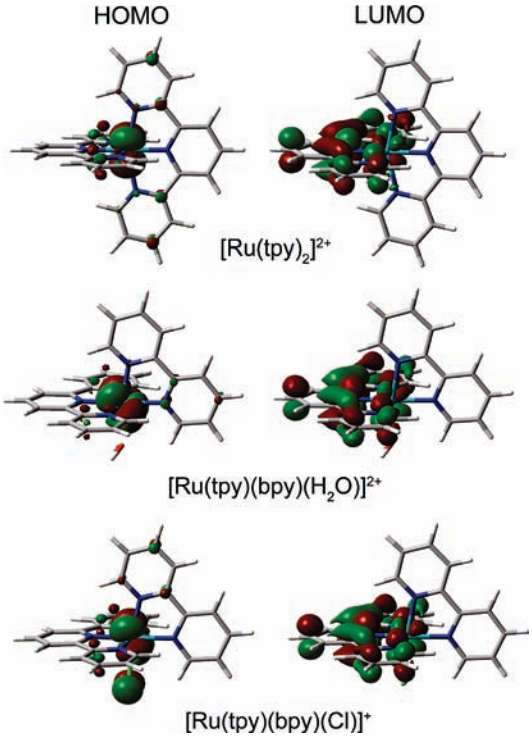

Figure 2. Frontier molecular orbitals of $[Ru(tpy)_2]^{2+}$, $[Ru(tpy)(bpy)(H_2O)]^{2+}$, and $[Ru(tpy)(bpy)(Cl)]^{+}$.

Frontier orbitals for the ground state of the three complexes in acetone are shown in Figure 2. The highest occupied molecular orbitals (HOMOs) of $[Ru(tpy)_2]^{2+}$ and $[Ru(tpy)(bpy)(H_2O)]^{2+}$ have a significant contribution from Ru t_{2g} d-orbital with a small π contribution from the polypyridine ligands. The HOMO of $[Ru(tpy)(bpy)(Cl)]^{+}$ consists mainly of an antibonding combination of a t_{2g} orbital on Ru metal and a p orbital on Cl^{-}. The lowest unoccupied molecular orbital (LUMO) for all complexes can be described as a π^* orbital on terpyridine ligands. The frontier orbitals in vacuum, dichloromethane, and water are identical to those displayed in Figure 2, except the LUMO of $[Ru(tpy)(bpy)(Cl)]^{+}$ in vacuum is localized on the bipyridine rather than the terpyridine ligand.

B. Singlet Excited States and Absorption Spectra. The experimental absorption spectra of the three complexes in

(33) Frisch, M. J.; Trucks, G. W.; Schlegel, H. B.; Scuseria, G. E.; Robb, M. A.; Cheeseman, J. R.; Montgomery, J. A.; Vreven, J., T. ; Kudin, K. N.; Burant, J. C.; Millam, J. M.; Iyengar, S. S.; Tomasi, J.; Barone, V.; Mennucci, B.; Cossi, M.; Scalmani, G.; Rega, N.; Petersson, G. A.; Nakatsuji, H.; Hada, M.; Ehara, M.; Toyota, K.; Fukuda, R.; Hasegawa, J.; Ishida, M.; Nakajima, T.; Honda, Y.; Kitao, O.; Nakai, H.; Klene, M.; Li, X.; Knox, J. E.; Hratchian, H. P.; Cross, J. B.; Bakken, V.; Adamo, C.; Jaramillo, J.; Gomperts, R.; Stratmann, R. E.; Yazyev, O.; Austin, A. J.; Cammi, R.; Pomelli, C.; Ochterski, J. W.; Ayala, P. Y.; Morokuma, K.; Voth, G. A.; Salvador, P.; Dannenberg, J. J.; Zakrzewski, V. G.; Dapprich, S.; Daniels, A. D.; Strain, M. C.; Farkas, O.; Malick, D. K.; Rabuck, A. D.; Raghavachari, K.; Foresman, J. B.; Ortiz, J. V.; Cui, Q.; Baboul, A. G.; Clifford, S.; Cioslowski, J.; Stefanov, B. B.; Liu, G.; Liashenko, A.; Piskorz, P.; Komaromi, I.; Martin, R. L.; Fox, D. J.; Keith, T.; Al-Laham, M. A.; Peng, C. Y.; Nanayakkara, A.; Challacombe, M.; Gill, P. M. W.; Johnson, B.; Chen, W.; Wong, M. W.; Gonzalez, C.; Pople, J. A. *Gaussian 03*, Revision D.02; Gaussian, Inc.: Wallingford, CT, 2004.

(34) Frisch, M. J.; Trucks, G. W.; Schlegel, H. B.; Scuseria, G. E.; Robb, M. A.; Cheeseman, J. R.; Scalmani, G.; Barone, V.; Mennucci, B.; Petersson, G. A.; Nakatsuji, H.; Caricato, M.; Li, X.; Hratchian, H. P.; Izmaylov, A. F.; Bloino, J.; Zheng, G.; Sonnenberg, L.; Hada, M.; Ehara, M.; Toyota, K.; Fukuda, R.; Hasegawa, J.; Ishida, M.; Nakajima, T.; Honda, Y.; Kitao, O.; Nakai, H.; Vreven, T.; Montgomery, J. A., Jr.; Peralta, J. E.; Ogliaro, F.; Bearpark, M.; Heyd, J. J.; Brothers, E.; Kudin, K. N.; Staroverov, V. N.; Kobayashi, R.; Normand, J.; Raghavachari, K.; Rendell, A.; Burant, J. C.; Iyengar, S. S.; Tomasi, J.; Cossi, M.; Rega, N.; Millam, J. M.; Klene, M.; Knox, J. E.; Cross, J. B.; Bakken, V.; Adamo, C.; Jaramillo, J.; Gomperts, R.; Stratmann, R. E.; Yazyev, O.; Austin, A. J.; Cammi, R.; Pomelli, C.; Ochterski, J. W.; Martin, R. L.; Morokuma, K.; Zakrzewski, V. G.; Voth, G. A.; Salvador, P.; Dannenberg, J. J.; Dapprich, S.; Daniels, A. D.; Farkas, O.; Foresman, J. B.; Ortiz, J. V.; Cioslowski, J.; Fox, D. J. *Gaussian 09*, Revision A.1; Gaussian, Inc.: Wallingford, CT, 2009.

(35) York, D. M.; Karplus, M. *J. Phys. Chem. A* **1999**, *103*, 11060–11079.

(36) Scalmani, G.; Frisch, M. J., in preparation **2009**.

acetone are shown in the top panel of Figure 3. The measured and calculated spectra in dichloromethane and water are provided as the Supporting Information. The measured absorption spectra of all three complexes are qualitatively similar, with intense $\pi \rightarrow \pi^*$ transitions at energies >350 nm. The broad, and in some cases structured, absorbance band around 400−500 nm corresponds to multiple MLCT transitions from Boltzmann-populated lowest-lying $d\pi^6(Ru) \rightarrow \pi^*(tpy, bpy)$.

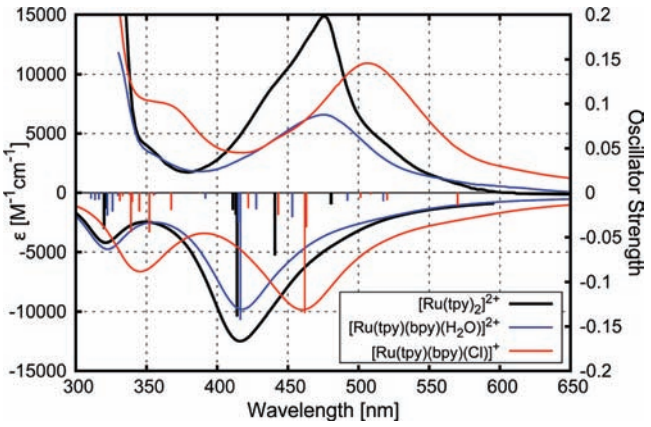

Figure 3. Experimental (top) and calculated (bottom) absorption spectra with the corresponding stick spectra of $[Ru(tpy)_2]^{2+}$, $[Ru(tpy)(bpy)(H_2O)]^{2+}$, and $[Ru(tpy)(bpy)(Cl)]^{+}$ in acetone. Each stick spectrum is composed of the δ-functions at the excitation energies obtained from TD-DFT calculations, with their intensities equal to the calculated oscillator strength.

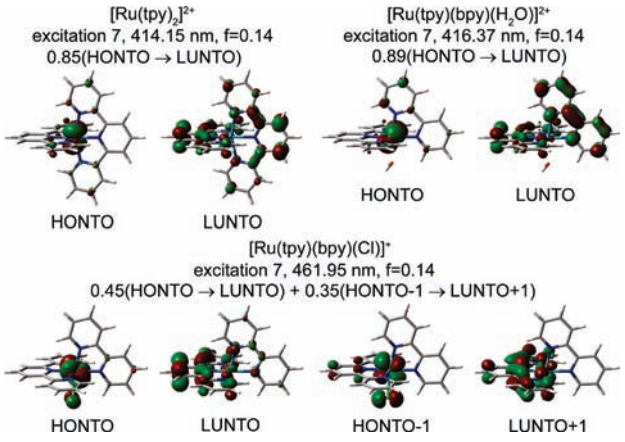

Figure 4. Natural transition orbitals for the most intense singlet excitations of $[Ru(tpy)_2]^{2+}$, $[Ru(tpy)(bpy)(H_2O)]^{2+}$, and $[Ru(tpy)(bpy)(Cl)]^{+}$ in acetone. HONTO = highest occupied natural transition orbital, LUNTO = lowest unoccupied natural transition orbital, f = calculated oscillator strength.

Substitution of Cl^- for H_2O in $[Ru(tpy)(bpy)(X)]^{n+}$ results in destabilization (i.e., energy rise) of the $d\pi(Ru)$ level through π-donation from Cl^-, which causes a decrease in the $d\pi \rightarrow \pi^*$ energy gap and therefore a significant red shift in the MLCT absorbance maximum.

The calculated spectra are shown in the bottom portion of Figure 3. The first 20 excitations were calculated to focus on the visible spectral region; therefore, the theoretical spectra do not include the excitations corresponding to the UV region. On the basis of the NTO analysis, the most intense peaks in the visible region correspond to MLCT $d \rightarrow \pi^*$ transitions. Figure 4 shows the lowest unoccupied and highest occupied natural transition orbitals for the singlet excitations of the three complexes, and their associated oscillator strengths (f).

Table 2 compares the calculated and experimental absorption maxima. While the error between the measured and calculated maxima (shown in Figure 3 and Table 2) ranges from 0.16 to 0.37 eV, the calculated results correctly reproduce the redshift in the absorption maxima (from $[Ru(tpy)_2]^{2+}$ and $[Ru(tpy)(bpy)(H_2O)]^{2+}$ to $[Ru(tpy)(bpy)(Cl)]^{+}$) in the measured spectra with the relative error of 0.12−0.16 eV, as well as the relative intensities and overall profile of the visible absorption bands.

C. Triplet Excited States and Emission Spectra. Emission spectra for $[Ru(tpy)(bpy)(H_2O)]^{2+}$ and $[Ru(tpy)(bpy)(Cl)]^{+}$ in acetone, dichloromethane, and water are shown in Figure 5. All emission data were obtained at room temperature, using excitation at 475−500 nm (see notes in Table 4). The spectra of both complexes display broad and structured bands that, as elucidated below, correspond to emission from a lowest-lying MLCT state (^{3}MLCT). Consistent with the absorption spectra, the emission maxima of the chloro complex in acetone and dichloromethane are markedly red-shifted relative to those of the aqua species. In addition to the main band above 700 nm, $[Ru(tpy)(bpy)(Cl)]^{+}$ displays a second band around 600 nm corresponding to the emission from $[Ru(tpy)(bpy)(H_2O)]^{2+}$. This additional emission from $[Ru(tpy)(bpy)(H_2O)]^{2+}$ is caused by a photoinduced substitution of Cl^- by H_2O, which occurs even with trace amounts of water. Consequently, we were unable to measure emission from $[Ru(tpy)(bpy)(Cl)]^{+}$ in water, as the H_2O completely displaced Cl^- through solvolysis, resulting in the emission spectrum of $[Ru(tpy)(bpy)(H_2O)]^{2+}$. The emission from $[Ru(tpy)_2]^{2+}$, while detectable in all solvents, was very weak at room temperature;

Table 2. Comparison of Experimental and Calculated (B3LYP/6-31G*,SDD) Absorption Maxima in the Visible Region[a]

		$[Ru(tpy)_2]^{2+}$	$Ru(tpy)(bpy)(H_2O)]^{2+}$	$[Ru(tpy)(bpy)(Cl)]^{+}$
dichloromethane	experimental [nm]	476	476	506
	calculated [nm]	419	418	462
	ΔE [eV]	0.35	0.36	0.23
acetone	experimental [nm]	476	476	506
	calculated [nm]	416	417	460
	ΔE [eV]	0.38	0.37	0.25
water	experimental [nm]	474	476	486
	calculated [nm]	419	420	454
	ΔE [eV]	0.34	0.36	0.18

[a] ΔE gives the energy difference between the calculated and experimental absorption maxima.

the band maximum is centered around 600−610 nm, but in acetone and dichloromethane shows a structured shoulder at ~ 665 nm.

To obtain simulated emission spectra, we have fully optimized the triplet excited states of $[Ru(tpy)_2]^{2+}$, $[Ru(tpy)(bpy)(H_2O)]^{2+}$, and $[Ru(tpy)(bpy)(Cl)]^{+}$ in dichloromethane, acetone, and water. Singly occupied natural orbitals for different triplet excited states in acetone are shown in Figure 6. Our results indicate that the triplet potential energy surfaces of these complexes are complicated, with ^{3}MC and ^{3}MLCT states lying close in energy. The ^{3}MC excited state is determined to be the lowest in energy for all three molecules. This is in accordance with a recent theoretical study,[12] which determined the energy difference between ^{3}MC and ^{3}MLCT states of $[Ru(tpy)_2]^{2+}$ to be only 4.0 kcal/mol in vacuum, with ^{3}MC being lower in energy.

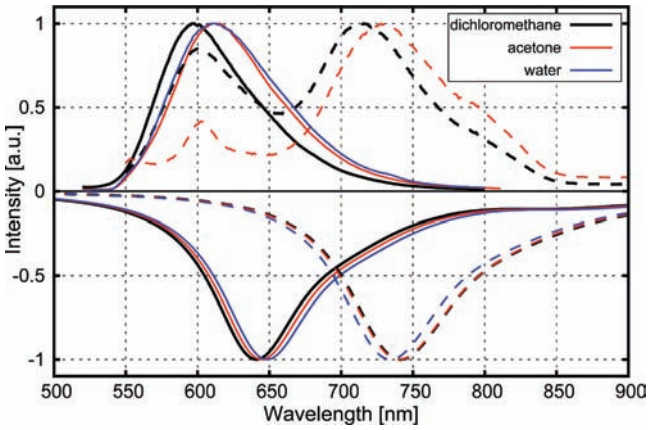

Figure 5. Experimental (top) and calculated (bottom) emission spectra for $[Ru(tpy)(bpy)(H_2O)]^{2+}$ and $[Ru(tpy)(bpy)(Cl)]^{+}$ in various solvents at room temperature. Solid lines represent experimental and simulated spectra for $[Ru(tpy)(bpy)(H_2O)]^{2+}$, while dashed lines belong to the $[Ru(tpy)(bpy)(Cl)]^{+}$. Bands in the region of 600−650 nm correspond to the emission from $[Ru(tpy)(bpy)(H_2O)]^{2+}$, and in 700−750 nm to $[Ru(tpy)(bpy)(Cl)]^{+}$.

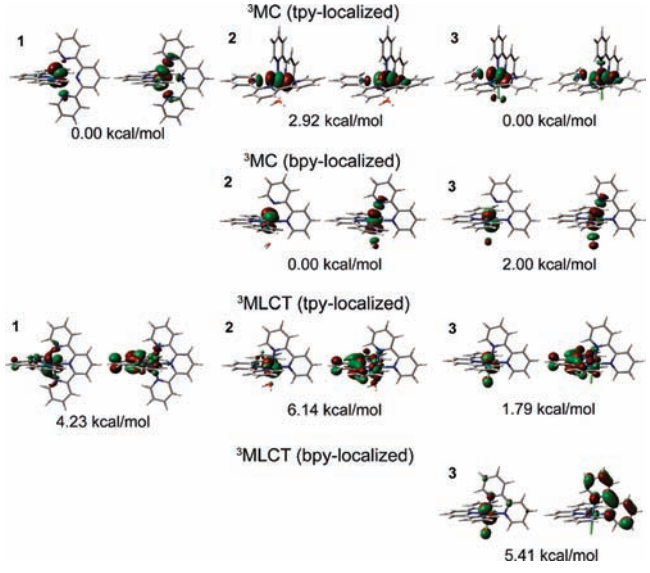

Figure 6. Singly occupied natural orbitals of different triplet excited states of $[Ru(tpy)_2]^{2+}$ (**1**), $[Ru(tpy)(bpy)(H_2O)]^{2+}$ (**2**), and $[Ru(tpy)(bpy)(Cl)]^{+}$ (**3**) in acetone.

Table 3 summarizes the energy differences between the lowest ^{3}MC and lowest ^{3}MLCT states of each complex in all three solutions considered. As can be seen in Table 3, the energy gap decreases with the increasing polarity of the solvent for $[Ru(tpy)_2]^{2+}$ and $[Ru(tpy)(bpy)(H_2O)]^{2+}$. Note that, in general, energy differences are within the accuracy of the computational methodology used, making it difficult to conclusively determine which one of the excited triplet states is the lowest in energy. Additionally, solvent effects are included in our calculations via the polarizable continuum model (PCM) rather than explicitly, which could have a significant effect on the ordering of the states when the differences are so small.

Interestingly, the largest energy gaps between the ^{3}MC and ^{3}MLCT states are seen for $[Ru(tpy)(bpy)(H_2O)]^{2+}$ (see Table 3). We believe that our calculations overestimate the stability of the bipyridine,H_2O-localized ^{3}MC state of this molecule, since the ligand water molecule is relatively free to move away from Ru center during the geometry optimization, thus favoring electron localization in the metal-centered σ^* orbital, rather than the ligand-centered π^* orbital. This is corroborated by a large increase (~0.5 Å) of Ru−O distance in bpy, H_2O-localized ^{3}MC state compared to the Ru−O distance in the ground state. In contrast, the Ru−Cl distance in bipyridine,Cl-localized ^{3}MC state increases by ~0.24 Å in comparison to the ground state Ru−Cl distance. Under realistic conditions, the freedom of movement of the H_2O ligand will be constrained by the solvent molecules and hydrogen bonding, which should destabilize the metal-centered σ^* orbital.

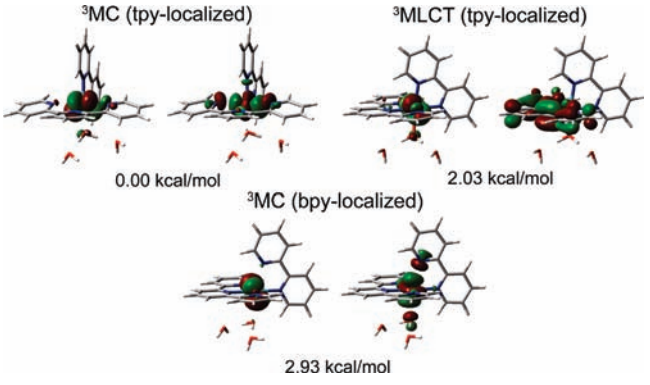

Figure 7. Singly occupied natural orbitals for different triplet excited states of $[Ru(tpy)(bpy)(H_2O)]^{2+}$ with explicit inclusion of the first hydration shell.

Table 3. Energy Differences (kcal/mol) between the Lowest ^{3}MC and Lowest ^{3}MLCT states in Different Solvents Calculated As $\Delta E = E(^3\text{MLCT}) - E(^3\text{MC})$[a]

	dichloromethane (ε = 8.93)	acetone (ε = 20.7)	water (ε = 78.39)	water + $2H_2O$ (ε = 78.39)
$[Ru(tpy)]^{2+}$	4.48	4.23	3.88	
$[Ru(tpy)(bpy)(H_2O)]^{2+}$	6.55	6.14	5.88	2.03
$[Ru(tpy)(bpy)(Cl)]^{+}$	1.58	1.79	1.76	

[a] $\Delta E > 0$ indicates that the ^{3}MC state is lower in energy than the ^{3}MLCT state.

Table 4. Comparison of Experimental and Calculated Emission Maxima for $[Ru(tpy)_2]^{2+}$, $[Ru(tpy)(bpy)(H_2O)]^{2+}$, and $[Ru(tpy)(bpy)(Cl)]^{+}$[a]

		$[Ru(tpy)_2]^{2+}$	$Ru(tpy)(bpy)(H_2O)]^{2+}$	$[Ru(tpy)(bpy)(Cl)]^{+}$
acetone	experimental [nm]	598[b]	612[g]	733[g]
	calculated [nm]	607	637	741
	ΔE [eV]	0.03	0.08	0.02
dichloromethane	experimental [nm]	611[c,e]	597[g]	720[f]
	calculated [nm]	607	632	741
	ΔE [eV]	0.01	0.12	0.05
water	experimental [nm]	c	610[g]	d
	calculated [nm]	607	640	734
	ΔE [eV]		0.10	

[a] ΔE gives the energy difference between calculated and experimental absorption maxima. [b] At 77K, from ref 11. [c] No emission observed at the room temperature. [d] Chloro- complex undergoes substitution in water; emission only observed at 612 nm. [e] Excitation at 475 nm; band is multistructured with shoulder at lower energy, near ~ 665 nm. [f] Excitation at 500 nm. [g] Excitation at 475 nm.

To confirm this, we have reoptimized the geometry of the ^{3}MC and ^{3}MLCT states of $[Ru(tpy)(bpy)(H_2O)]^{2+}$, where we explicitly included the two H_2O molecules of the first solvation shell, hydrogen-bonded to the H_2O ligand and included the remaining solvent effects through the PCM model (see Figure 7). The explicit addition of the two solvent molecules significantly decreased the energy differences between the ^{3}MC and ^{3}MLCT states, with the ^{3}MLCT now being lower in energy than the bipyridine, H_2O-localized ^{3}MC state by 0.9 kcal/mol. The terpyridine-centered ^{3}MC state is still lower in energy than the ^{3}MLCT state by 2.0 kcal/mol, although the energy difference decreased by 1.3 kcal/mol.

These results suggest that similar solvent effects might also destabilize the terpyridine-centered ^{3}MC state. This ^{3}MC state is characterized by the electron localization in a σ^* orbital, leading to the noticeable deformation of the terpyridine ligand as it opens up to increase the Ru−N distances by ~ 0.3 Å in the direction of the $\sigma_{d\text{-}p}$ bond. It is likely that the deformation and opening of the terpyridine ligand will be hindered by the crowding of the solvent molecules around the terpyridine group. To confirm this, one would need to perform calculations on a fully solvated $[Ru(tpy)(bpy)(H_2O)]^{2+}$ molecule, which is a very computationally demanding task. Also, similar solvation effects will influence the relative stabilities of the ^{3}MC and ^{3}MLCT states of $[Ru(tpy)_2]^{2+}$ and $[Ru(tpy)(bpy)(Cl)]^{+}$ complexes.

The terpyridine-localized ^{3}MLCT excited states were used to simulate the emission spectra for all three complexes, which are shown in Figure 5. Comparison of calculated and theoretical emission maxima is given in Table 4. The emission maxima are overall in a very good agreement with the maxima determined by the experimental measurements, with calculated maxima shifted by 0.03−0.12 eV to lower energies.

Conclusions

In this work we studied the spectroscopic properties and electronic structure of $[Ru(tpy)(bpy)(H_2O)]^{2+}$, $[Ru(tpy)_2]^{2+}$, and $[Ru(tpy)(bpy)(Cl)]^{+}$ in dichloromethane, acetone, and water. All three complexes display strong absorption peaks in the visible region, which were assigned based on TD-DFT calculations to the MLCT transitions from Ru d(t_{2g}) orbital into a π^* orbital on the terpyridine ligand. The absorption spectra obtained with TD-DFT calculations are in a good agreement with the experimental data.

The emission spectra of the three complexes were also studied, both experimentally and computationally, and are determined to arise from a terpyridine-localized ^{3}MLCT state. Computational results suggest that a ^{3}MC is the lowest energy triplet excited state for all three complexes in the solutions investigated. However, computed energy differences between the ^{3}MC and ^{3}MLCT states are between 1.6 and 4.5 kcal/mol (within the error of the computational methodology), preventing a conclusive assignment of the lowest triplet excited state on the basis of calculations alone.

An important finding is that the energy gap between the lowest ^{3}MC and ^{3}MLCT states is influenced by the solvent environment and decreases with the increasing solvent polarity, indicating that the solvent effects induce the stabilization of the ^{3}MLCT state. Our theoretical results also provide evidence that the inclusion of the solvent effects explicitly, rather than through the use of the PCM, should promote further stabilization of the ^{3}MLCT state relative to the ^{3}MC states.

Acknowledgment. We would like to thank Drs. Gabriel Montano and Andrew Dattelbaum for help with emission measurements and Dr. Sergei Tretiak for providing us with a program for computing the Huang−Rhys factors. This work was supported by the Laboratory Directed Research and Development (LDRD) program at Los Alamos National Laboratory. Los Alamos National Laboratory is operated by Los Alamos National Security, LLC, for the National Nuclear Security Administration of the U.S. Department of Energy under contract DE-AC52-06NA25396.

Supporting Information Available: Calculated and experimental absorption spectra in dichloromethane and acetone; geometries of all calculated stationary points in Ångströms. This material is available free of charge via the Internet at http://pubs.acs.org.